J. Phys. Earth, **37**, 101–131, 1989

CRUSTAL MOVEMENTS IN THE INNER ZONE OF SOUTHWEST JAPAN ASSOCIATED WITH STRESS RELAXATION AFTER MAJOR EARTHQUAKES

Takao TABEI*

Geophysical Institute, Kyoto University, Kyoto, Japan

(Received May 30, 1988; Revised April 7, 1989)

Transient deformation resulting from postseismic stress relaxation in underlying viscoelastic layers is examined. The main purpose of the present study is to understand spatial and temporal modes of postseismic deformation especially due to strike-slip faulting with a realistic geometry. The fault size as well as the viscoelastic structure of the earth proved to have large effects on the amount of postseismic deformation. Therefore, it should be taken into serious consideration in modeling the faulting. It is noteworthy that the concentration of shear strain into the near field continues long after the faulting. This strain concentration is similar to the preseismic strain accumulation and is contrary to the coseismic strain release. The viscoelastic structure of the earth, however, is hard to determine solely by the surface measurements performed at long time intervals. Crustal movements in the Inner Zone of Southwest Japan, in particular, those associated with the 1927 Tango earthquake of $M=7.5$, are then investigated in connection with postseismic stress relaxation. The discrepancies between the observed and calculated postseismic deformations can be reduced if the effect of tectonic stress is added to the calculated deformation field.

1. *Introduction*

It is widely accepted that the basic model to explain the physical behavior of the earth's crust and upper mantle generally consists of three layers with different rheological properties; namely, the uppermost elastic and brittle lithosphere, the intervenient ductile asthenosphere with low viscosity, and the substratum with relatively high viscosity. In addition, it is also recognized that there exist considerable regional heterogeneities in both thicknesses and properties of the layered structure of the earth. These heterogeneities probably characterize the mode of accumulation and release of tectonic stress in the region, and this mode is reflected in the crustal movements and seismic activity peculiar to the region.

* Present address: Department of Physics, Faculty of Science, Kochi University, Kochi, Japan.

With the recent advance in accuracy in the determination of hypocenters of earthquakes, it has become clear that there is a sharp cut-off depth for seismic activities in tectonically active inland regions (e.g., KOBAYASHI, 1976; OIKE, 1977; SIBSON, 1982; MEISSNER and STREHLAU, 1982; CHEN and MOLNAR, 1983; MIKUMO *et al.*, 1988; ITO, 1988). It seems that most earthquakes that occur inland sufficiently far from the subduction zone are restricted to the upper crust, in other words, a seismic-aseismic transition occurs at the mid-crustal depth. The thermal dependence of fracture strength of rock has been discussed to interpret the lower limit of focal depth in Central and Southwest Japan (e.g., KOBAYASHI, 1976; MIKUMO *et al.*, 1988; ITO, 1988). Based on laboratory data on rock deformations, SIBSON (1982) assumed frictional failure and quasi-plastic flow in the upper and lower crusts, respectively, and clarified the depth-dependence of shear resistance of the continental crust in the Western United States. These studies suggest that an anelastic treatment is indispensable not only for the upper mantle but for the lower crust when the failure and deformation of the crust in tectonically active inland regions are discussed.

Transient crustal movements following an elastic rebound at the time of a large earthquake are interesting phenomena in understanding the anelastic properties of the earth's crust and upper mantle and also in comprehending the mode of accumulation and release of tectonic stress. NUR and MAVKO (1974) first obtained analytical expressions of the postseismic displacement fields due to a dislocation in an elastic layer overlying a viscoelastic half-space. In recent years, further studies have been carried out on quasi-static surface deformation resulting from postseismic stress relaxation in underlying viscoelastic layers.

Crustal movements due to major underthrust earthquakes occurring repeatedly at the subduction zone are characterized by large vertical displacements whose patterns significantly change with time. They have mostly been modeled in connection with a steady plate subduction and asthenospheric stress relaxation (e.g., THATCHER and RUNDLE, 1979; THATCHER *et al.*, 1980; MIYASHITA, 1983; THATCHER and RUNDLE, 1984; MIYASHITA, 1987) and a relatively simple two- or three-layered structure model seems to explain appropriately the transient crustal movements observed.

Similar modelings have also been made for slow and steady deformation along a strike-slip fault (RUNDLE and JACKSON, 1977; SAVAGE and PRESCOTT, 1978; YANG and TOKSÖZ, 1981). These modelings, however, have mainly been made for a highly idealized long fault that exists in an elastic layer overlying a viscoelastic substratum. Thus, it is questionable whether the model results are immediately applicable to crustal movements due to moderate-size faulting. For example, an earthquake with a magnitude larger than 7.0 that occurs in the Inner Zone (the Japan Sea side) of Southwest Japan is mainly represented by strike-slip faulting with a length of about 30 to 40 km. However, quantitative consideration has not yet been given for postseismic deformations caused by stress relaxation after such faulting.

In the present study, the effects of fault size and viscoelastic structure of the earth's crust and upper mantle on the postseismic deformations are examined

through a three-dimensional numerical simulation in which viscoelastic treatments are introduced for the lower crust and the upper mantle on the basis of the vertical distribution of microearthquakes. The spatial pattern, amount, and time-dependence of the deformation are then estimated for faulting with a realistic geometry. The deformation due to postseismic stress relaxation is formulated according to MATSU'URA *et al.* (1981) and IWASAKI (1985). In their formulations, quasi-static deformations caused by faulting with arbitrary orientation and slip-vector in a multi-layered half-space can be treated. Furthermore, crustal movements observed during several decades after the 1927 Tango earthquake of $M=7.5$, that occurred in the Inner Zone of Southwest Japan, are investigated especially in connection with the relation between the postseismic stress relaxation in underlying viscoelastic layers and the tectonic stress. These investigations will give us a new insight into crustal movements related to the mode of accumulation and release of tectonic stress.

2. *Modeling of Postseismic Deformation*

2.1 Tectonic setting of the Inner Zone of Southwest Japan

Figure 1 shows the distribution of the main active faults and tectonic lines in and around Southwest Japan (THE RESEARCH GROUP FOR ACTIVE FAULTS, 1980). The Median Tectonic Line separates Southwest Japan into two tectonic regions, namely, the Inner Zone (the Japan Sea side) and the Outer Zone (the Pacific side).

Tectonics in the Outer Zone is characterized by an interaction between the Philippine Sea and Eurasian plates. The former is considered to be subducting northwestward beneath Southwest Japan from the Nankai trough (Fig. 1). Along this trough, great earthquakes have repeatedly occurred accompanied by large crustal movements in the coastal regions (ANDO, 1975). Studies of the focal mechanisms of these earthquakes and their aftershocks show that these are the earthquakes of low-angle thrust type (ICHIKAWA, 1971; KANAMORI, 1972 a; SHIONO, 1977).

The tectonic setting is rather complicated in the Inner Zone. The regular arrangement of reverse faults and conjugate strike-slip faults shown in Fig. 1 suggests that they have been formed by a horizontal tectonic compression in a nearly E-W direction (HUZITA *et al.*, 1973). Similarly, studies of focal mechanisms of shallow earthquakes in this region have revealed that pressure axes lie in a horizontal E-W to ESE-WNW direction (ICHIKAWA, 1971; NISHIDA, 1973; SHIONO, 1977), some examples of which are shown in Fig. 2. Moreover, long-term crustal movements detected by geodetic measurements indicate a nearly E-W contraction (GEOGRAPHICAL SURVEY INSTITUTE, 1987). It is therefore considered that the tectonic stress acting in the Inner Zone is dominantly the horizontal compression in the almost E-W direction and the movement of the Philippine Sea plate is not a governing factor (e.g., HASHIMOTO, 1982). The detailed mechanism causing such an E-W compression, however, has not been clarified yet and is under lively discussion.

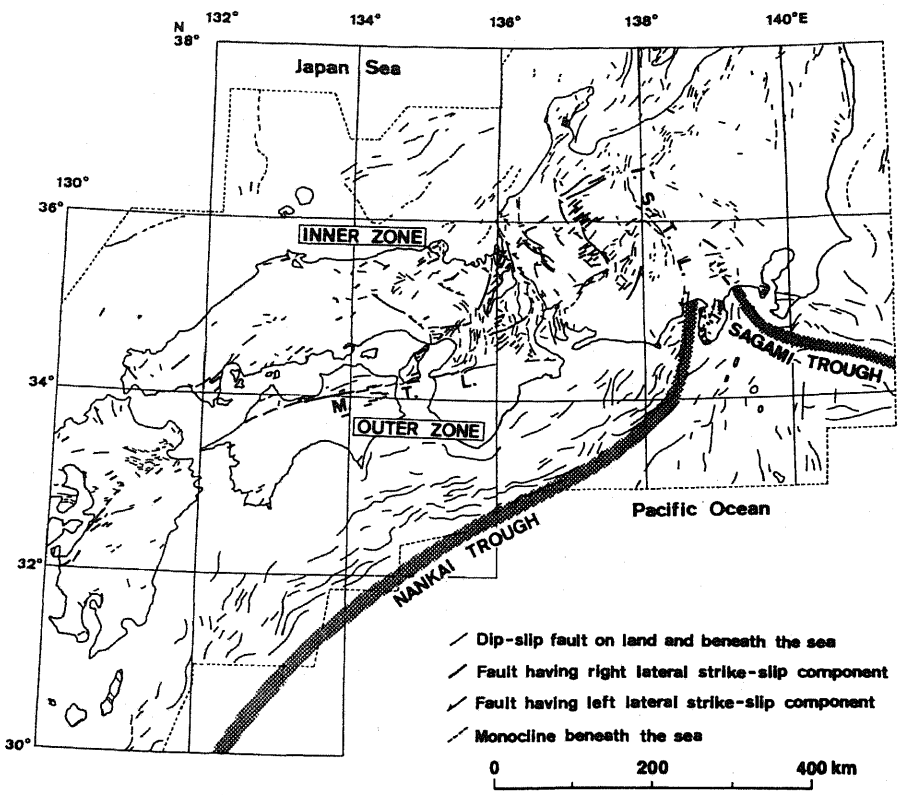

Fig. 1. A map showing the distribution of the main active faults and tectonic lines in and around Southwest Japan (compiled from THE RESEARCH GROUP FOR ACTIVE FAULTS, 1980). M.T.L. and I.S.T.L. represent the Median Tectonic Line and the Itoigawa-Shizuoka Tectonic Line, respectively.

Three large earthquakes in the Inner Zone, namely, the 1927 Tango ($M=7.5$), the 1943 Tottori ($M=7.4$), and the 1948 Fukui ($M=7.3$) earthquakes, were accompanied by remarkable crustal movements showing typical strike-slip faulting (TSUBOI, 1932; NASU, 1950; SATO, 1973). Their focal mechanisms are indicated in Fig. 2 by symbols **Ta**, **To**, and **Fu**, respectively. KANAMORI (1972 b, 1973) calculated the synthetic seismograms for the three earthquakes on the basis of the distribution of P-wave first motions, the aftershock distributions, and the triangulation data. He determined fault parameters from the best-fit synthetic seismograms. The results obtained are listed in Table 1. The three earthquakes are very similar in scale and type of faulting and can be regarded as representing typical patterns of the release of tectonic stress that has been accumulated in this region.

Shallow microseismicities in the Inner Zone are considerably active along the active faults, as shown in Fig. 3(a) (OIKE, 1977). The vertical distribution of

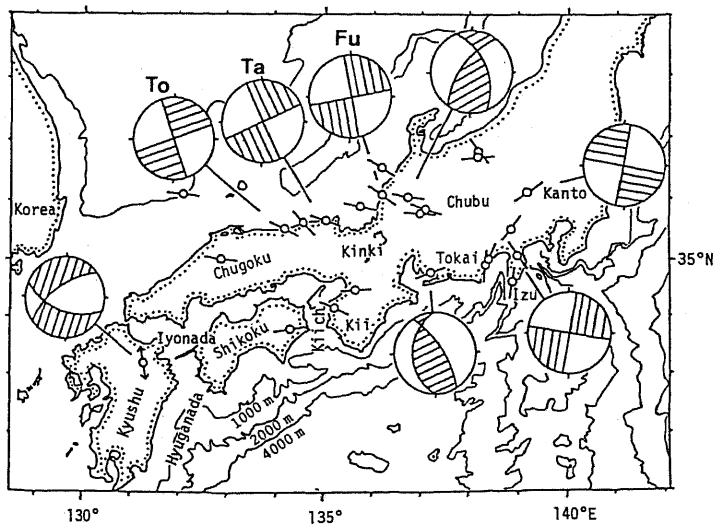

Fig. 2. Distribution of P-axes and focal mechanisms of major crustal earthquakes in Southwest Japan (after SHIONO, 1977). All diagrams are projected on the lower hemisphere. Shaded and open quadrants of the diagrams indicate the compressional region of P-wave first motion and the dilatational one, respectively. Symbols **Ta**, **To**, and **Fu** represent the 1927 Tango ($M=7.5$), the 1943 Tottori ($M=7.4$), and the 1948 Fukui ($M=7.3$) earthquakes, respectively.

Table 1. Fault parameters of the three large earthquakes in the Inner Zone of Southwest Japan (after KANAMORI, 1972b, 1973).

Earthquake	M	M_0*	L (km)	W (km)	U_0 (m)	$\Delta\sigma$ (bar)	Type**
Tango (1927)	7.5	4.6	35	13	3.0	100	L
Tottori (1943)	7.4	3.6	33	13	2.5	83	R
Fukui (1948)	7.3	3.3	30	13	2.0	83	L

* In units of 10^{26} dyn·cm. ** R, Right-lateral strike-slip; L, left-lateral strike-slip.

accurately determined hypocenters of microearthquakes indicates a sharp concentration of focal depths into the upper crust and an abrupt disappearance in and below the lower crust, as shown in Fig. 3(b). These results as well as the distribution of active faults give important clues for understanding the nature of the crust of the tectonically active inland region. For example, we can consider that strain buildup caused by accumulation of tectonic stress and strain release through brittle fractures alternately take place in the elastic upper crust, while an acting stress is continuously consumed by an anelastic flow in or below the lower crust, and consequently, stress is not accumulated there.

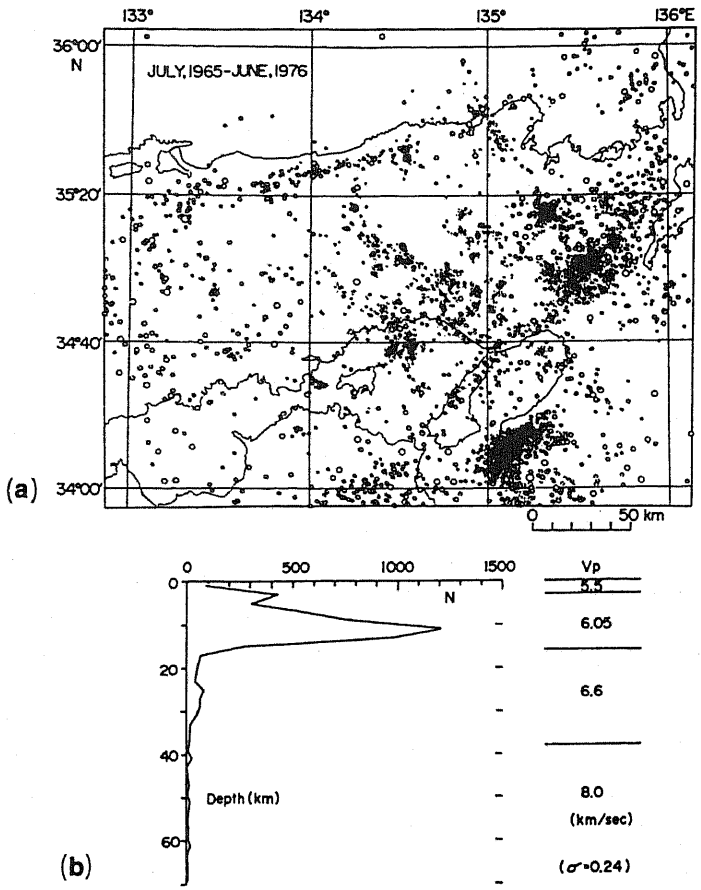

Fig. 3. Distribution of microearthquakes that occurred during the period from July 1965 to June 1976 (after OIKE, 1977). (a) Epicentral distribution of shallow microearthquakes whose depths are less than 40 km. (b) Representative crustal structure and vertical distribution of hypocenters in the same region as that shown in (a).

2.2 *Mathematical formulation*

Transient deformation induced by postseismic stress relaxation in underlying viscoelastic layers is modeled according to the formulations by MATSU'URA *et al.* (1981) and IWASAKI (1985).

Figure 4(a) shows a layered half-space that consists of n parallel layers overlying substratum (the $(n+1)$-th layer), where the n-th layer and the substratum are assumed to be viscoelastic (behaving as an elastic solid for confining pressure and as a Maxwell substance for stress deviation) and the other layers are perfectly elastic. The viscosities of the n-th layer and the substratum are denoted by η' and η, respectively. Coordinates and fault geometry are shown in Fig. 4(b).

When the source time function can be represented by the Heaviside step

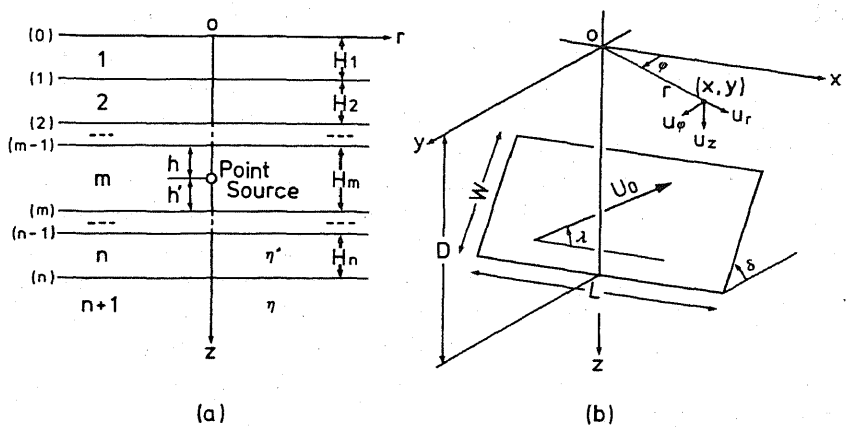

Fig. 4. Definition of parameters (modified from IWASAKI, 1985). (a) Numbering of layers and their interfaces. η and η' denote the viscosities of the substratum and the n-th layer, respectively. (b) Geometry of the finite-dimensional fault. L, Fault length; W, fault width; D, depth to the lower margin of the fault; δ, dip-angle; U_0, amount of final dislocation; λ, slip-angle of the hanging wall against the foot one; and $u_{r(\varphi,z)}$, displacement components in cylindrical coordinates.

function $H(t)$, total displacement fields at the surface are written in the cylindrical coordinates as

$$w_{r(\varphi,z)}(r, \varphi, t)=u_{r(\varphi,z)}(r, \varphi)\cdot H(t)+v_{r(\varphi,z)}(r, \varphi, t)\,, \tag{1}$$

where $u_{r(\varphi,z)}$ represents the coseismic elastic displacement and $v_{r(\varphi,z)}$ the postseismic viscoelastic one that is dependent on the elapsed time after faulting. When a point dislocation is given in the m-th layer, the radial component v_r of the viscoelastic displacements is expressed in the integral representation as

$$\begin{aligned} v_r(r, \varphi, t)=\frac{U_0}{4\pi}H(t)\sum_{l=0}^{2}\Bigg[& K_l(\varphi)\int_0^\infty \{V_{r,1}(t, \xi)\mathrm{e}^{-h\xi}+(-1)^l V_{r,2}(t, \xi)\mathrm{e}^{-h'\xi}\}\frac{\partial J_l(\xi r)}{\partial r}\mathrm{d}\xi \\ & -L_l(\varphi)\int_0^\infty \{V_{r,3}(t, \xi)\mathrm{e}^{-h\xi}+(-1)^l V_{r,4}(t, \xi)\mathrm{e}^{-h'\xi}\}\frac{\partial J_l(\xi r)}{\partial r}\mathrm{d}\xi \\ & +\alpha_m h' L_l(\varphi)\int_0^\infty \xi\{V_{r,1}(t, \xi)\mathrm{e}^{-h\xi}-(-1)^l V_{r,2}(t, \xi)\mathrm{e}^{-h'\xi}\}\frac{\partial J_l(\xi r)}{\partial r}\mathrm{d}\xi\Bigg] \\ & -\frac{U_0}{4\pi}H(t)\sum_{l=1}^{2}\frac{\partial^2 L_l(\varphi)}{\partial\varphi^2}\int_0^\infty \{V_{\varphi,1}(t, \xi)\mathrm{e}^{-h\xi}-(-1)^l V_{\varphi,2}(t, \xi)\mathrm{e}^{-h'\xi}\}\frac{J_l(\xi r)}{r}\mathrm{d}\xi\,, \end{aligned} \tag{2}$$

with

$$\left.\begin{aligned} \alpha_m &= (\lambda_m+\mu_m)/(\lambda_m+2\mu_m)\,, \\ h' &= H_m-h\,, \end{aligned}\right\} \tag{3}$$

where U_0 is the amount of dislocation, $J_l(\xi r)$ the Bessel function of order l, λ_m and μ_m the Lamé's constants of the source-existing m-th layer, and K_l and L_l the geometrical functions depending on the station azimuth (φ) and the dip-angle (δ) and slip-angle (λ) of the fault. The other two displacement components, v_φ and v_z, are expressed in the forms similar to Eq. (2).

$V_{r,j}$, $V_{\varphi,j}$, and $V_{z,j}$, which are included in the integrals in Eq. (2), are referred to as the viscoelastic kernel functions. They represent the time-dependence of the deformation, which is affected by both the layered structure and the source time function. However, they are not related to the fault geometry. The gravitational effect is incorporated in them (IWASAKI and MATSU'URA, 1982). The kernel functions are approximated by analytical functions using a technique developed by MATSU'URA *et al.* (1981) so that the semi-infinite integrals with respect to ξ in Eq. (2) can be numerically evaluated.

For displacement fields due to a finite-dimensional fault, numerical double integrations of the solutions obtained for a point source must be carried out over a fault plane with length L and width W (Fig. 4(b)). In the present study, the integrations are carried out using a new method of two-dimensional interpolation by bi-cubic B-spline functions. First, grid points are selected on the fault plane as the location of point sources. Taking the location of point source as a two-dimensional discrete valuable, displacement at a position at the surface is calculated. Then calculated displacements are interpolated and represented by bi-cubic B-spline functions. Consequently, double integration can be reduced to the numerical integration of the analytical bi-cubic functions. In the present study, the number of grid points has usually been taken as 84 (12 and 7 in length and width directions, respectively). For the calculation of the near field, however, more grid points have been selected to enhance the accuracy of interpolation. Though this method of integration requires rather a long computational time, it has a high degree of accuracy and is, without any modification, applicable to the case of the non-uniform distribution of dislocation on the fault plane.

2.3 Structure model of the earth's crust and upper mantle

The postseismic viscoelastic deformation at the surface is dependent on the layered structure of the earth's crust and upper mantle.

On the basis of the delay in arrival time of long-traveled seismic waves, the upper mantle beneath the Japanese Islands has been thought to have the characteristics of low velocity and large attenuation (KANAMORI, 1970). The three-dimensional attenuation structure of Northeast Japan, which was estimated by the inversion of seismic intensity data, shows that the low-Q zones are dominant in the crust and upper mantle on the backarc side and are in contrast with the high-Q zones on the Pacific side (HASHIDA and SHIMAZAKI, 1987). Moreover, a numerical modeling of tectonic flow induced by a subducted slab has indicated high temperature and low viscosity beneath island arcs and marginal basins (ANDREWS and SLEEP, 1974). Therefore, the idea that the asthenosphere beneath the Japanese

Table 2. Structure model for the Inner Zone of Southwest Japan.

Layer	H (km)	V_P (km/s)	Poisson's ratio	ρ (g/cm^3)	Viscosity
1	18	6.10	0.226	2.67	—
2	17	6.65	0.258	3.00	η'
3	—	7.92	0.283	3.42	η

Islands has been highly developed is well founded. This idea is also supported by the structure model of P-wave velocity derived from the explosion seismic observation (YOSHII *et al.*, 1974).

In the present study, we assume that a thick asthenosphere with low viscosity underlies the inland crust of Southwest Japan, and the effect of the substratum with its relatively high viscosity is negligible compared with that of the asthenosphere. In addition, we introduce a viscoelastic treatment into the lower crust on the basis of vertical distribution of microearthquakes shown in Fig. 3(b). Therefore, the present structure model for the Inner Zone of Southwest Japan consists of the elastic upper crust, the viscoelastic lower crust with its relatively high viscosity, and the substratum (upper mantle), which is recognized as an asthenosphere with low viscosity and sufficient thickness. A similar viscoelastic treatment of the lower crust and upper mantle has been made in a finite-element modeling of Northeast Japan by SATO *et al.* (1981).

Table 2 lists the material constants of the structure model employed in the present study. The thicknesses and P-wave velocities of the layers are mostly derived from the result of explosion seismic observations (YOSHII *et al.*, 1974). The Poisson's ratios and densities are mainly from SATO *et al.* (1981). The calculations of time-dependent postseismic deformation are executed varying the viscosity ratio η'/η. The elapsed time after faulting is measured in units of the Maxwell's relaxation time of the upper mantle, η/μ_3, where μ_3 represents its rigidity. The η/μ_3 will be denoted by τ here.

The model employed here ignores the lateral heterogeneities of the structure. These possibly result mainly from the presence of a long subducted slab and induce an additional surface deformation. The seismic plane of subcrustal earthquakes (MIZOUE, 1976) and the large-scale three-dimensional seismic velocity structure (HIRAHARA, 1981) beneath Southwest Japan indicate that the configuration of the subducted Philippine Sea plate is complex and the subduction is not uniform. NAKANISHI (1980) has reported that ScSp phases were observed at several stations in the Shikoku and Chugoku regions (Fig. 2), which were interpreted as converted waves from ScS to P at the dipping interface in the upper mantle. He has pointed out the possibility that this interface is the upper boundary of the subducted Philippine Sea plate that had reached beneath the Chugoku region. At the same time, however, he has indicated another possibility that this interface is related to the aseismic dead slab that had intermittently descended in the past subduction process

because no subcrustal earthquake occurs beneath the Chugoku region. The absence of subcrustal seismicity implies that at present the interaction between the subducted Philippine Sea plate and the continental Eurasian plate is not so strong beneath the Chugoku region. As a first approximation, therefore, ignoring the effects of subducted slab may be justified for modeling the deformations in the Inner Zone of Southwest Japan.

The effect of the superficial layer of the crust on the surface deformation is not taken into account in the present model because it is exceedingly hard to quantify. TANAKA (1981) has concluded that some of the postseismic deformations detected by strainmeters or tiltmeters, which were represented by exponential functions with time constants of a few years, may be caused by an earthquake-induced viscoelastic relaxation of stress within rocks around the observation vault. We recognize that the local crustal movements are sometimes largely affected by heterogeneities within rocks, transient movement of underground water, instabilities of alluvial layers, and so forth. However, it is uncertain whether the superficial layer of the crust has a governing factor in long-term regional crustal movements.

3. *Model Results*

3.1 *Effect of fault size*

In studies of the problem of elastic-viscoelastic coupling, an idealized two-dimensional treatment such that the fault has an infinite length is often adopted for simplification. However, we are convinced that the fault size may be one of the major factors governing the coseismic and postseismic deformation fields. Here we evaluate the effect of variation of fault length on both the elastic and viscoelastic deformations. The structure model presented in Table 2 is employed in the evaluation.

Holding that the fault width, dip-angle, and slip-vector on the fault plane are fixed, elastic and viscoelastic displacements are calculated for several cases with different fault lengths. Figure 5 shows the changes in profiles of horizontal displacement parallel to the strike of vertical strike-slip fault. The profiles are taken along the line perpendicular to the center of the fault at the surface. The displacement amplitude is normalized by the amount of coseismic dislocation on the fault plane. The width of fault is fixed at 15 km. Figure 6 shows the changes in vertical displacement profiles for a dip-slip fault, where the width and dip-angle are fixed at 30 km and 30°, respectively. The viscosity ratio η'/η in both Figs. 5 and 6 is tentatively taken as 10.

In general, the variation in fault length has a larger effect on the viscoelastic deformation than the elastic one, and this is more remarkable in dip-slip faulting than in strike-slip faulting, as seen from Figs. 5 and 6. At the early stage of the postseismic deformation (lower left panels in Figs. 5 and 6, where the elapsed time after faulting is twice the relaxation time of the asthenosphere), differences among the displacement profiles are not clearly distinguishable because of their small

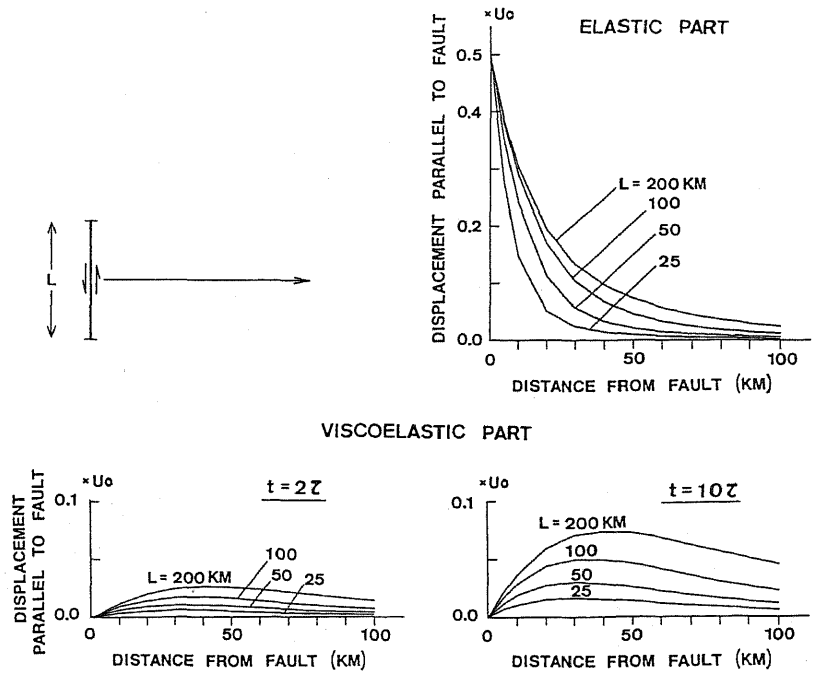

Fig. 5. Changes in horizontal displacement profiles with length of a pure strike-slip fault. The fault is vertical and its width is fixed at 15 km. Displacements parallel to the fault strike are plotted, where the scale of displacement is normalized by U_0 that is the amount of coseismic dislocation on the fault plane. The profiles are taken along the line extending on the surface perpendicularly to the center of the fault. In the postseismic viscoelastic deformation (lower two figures), the viscosity ratio η'/η is assumed to be 10.

amplitudes. On the other hand, the effect of variation in fault length becomes more remarkable gradually with time (lower right panels in Figs. 5 and 6). Therefore, we conclude that the fault length should be taken into serious consideration in modeling the long-term postseismic viscoelastic deformation.

3.2 Spatial patterns of displacement and strain fields

To understand the time-dependent deformation due to moderate-size strike-slip faulting, displacement and strain fields are calculated at several elapsed times after faulting. The model fault is assumed to be vertical and have a length of 34 km and a width of 13 km. The upper margin of the fault must be located underground because singular points appear if a source is located at the surface. Thus the depth to the lower margin of the model fault is tentatively taken as 13.13 km; that is 1% larger than the fault width. The fault geometry is nearly equivalent to those of the 1927 Tango, the 1943 Tottori, and the 1948 Fukui earthquakes.

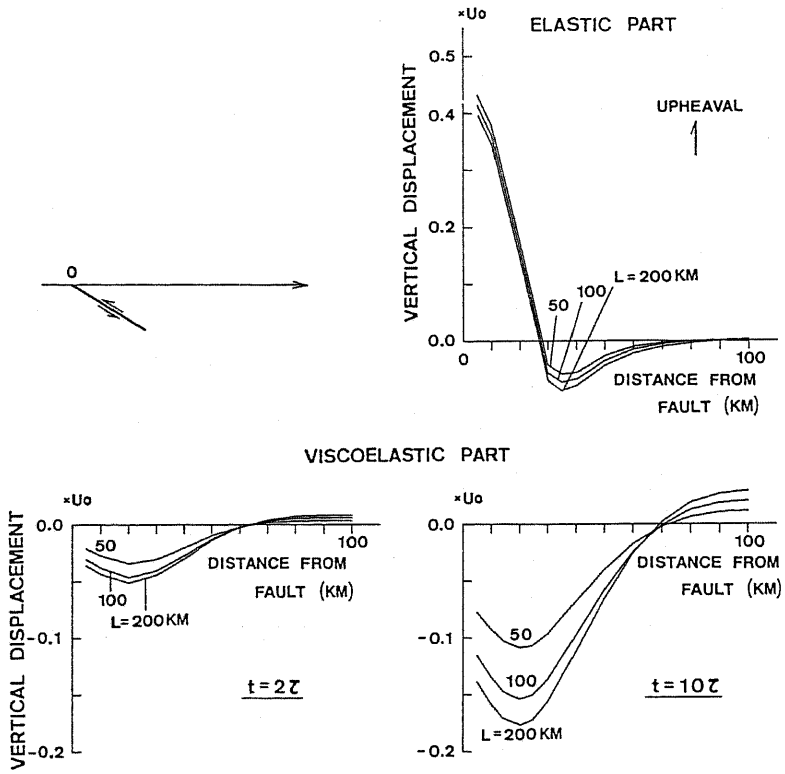

Fig. 6. Changes in vertical displacement profiles with length of a pure dip-slip fault. The fault width and dip-angle are fixed at 30 km and 30°, respectively. The profiles are taken along the same line as in Fig. 5. The viscosity ratio is assumed to be 10.

A dislocation with a pure left-lateral strike-slip component of 1 m has been uniformly given on the fault plane. Horizontal displacements, vertical displacements, and horizontal strains are calculated and shown in Figs. 7, 8, and 9, respectively. The coseismic elastic deformations and the postseismic viscoelastic ones are shown in (a) and (b) in each figure, respectively. Here, the viscoelastic deformations are represented by those at the elapsed time $t=10\tau$. The viscosity ratio η'/η is assumed to be 10.

As shown in Fig. 7(a) and (b), the horizontal postseismic displacement vectors are generally in the same sense as the coseismic ones. The amounts of displacements, however, are quite different in Fig. 7(a) and (b). It seems that the surrounding region is remarkably displaced in order to compensate for the relatively small displacements at the time of faulting. However, the cumulative amounts of postseismic displacements are not particularly large.

The positions where the maximum vertical displacement appears do not

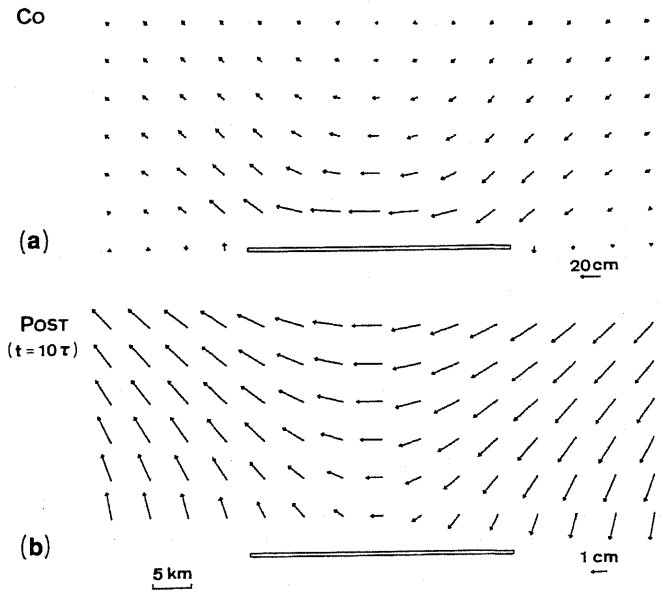

Fig. 7. Horizontal displacement due to pure strike-slip faulting with a vertical fault plane. The length and width of the fault are assumed to be 34 and 13 km, respectively. The depth ot the lower margin of the fault is taken 1% larger than the fault width. A uniform dislocation with a left-lateral component of 1 m is given on the fault plane. (a) Coseismic displacements. (b) Postseismic displacements at the elapsed time $t=10\tau$. The viscosity ratio is assumed to be 10.

coincide in Fig. 8(a) and (b). These figures show the turnover from coseismic upheavals to postseismic subsidences and the reverse case from coseismic subsidences to postseismic upheavals. These turnovers may be caused by the slow reaction of the underlying viscoelastic layers against the sudden change in stress fields and by the compensation for the undulation of the boundary between the elastic and viscoelastic layers. The gravitational effect has been considered in calculation of postseismic deformations, although it proves not dominant in this case.

The most noteworthy result is obtained from the pattern of the strain field. As shown in Fig. 9(a) and (b), the postseismic strains in the near field of the fault are generally accumulated in the reverse sense to those of the coseismic strain releases. In other words, the pattern of postseismic strains is roughly similar to the distribution of shear strains that were accumulated in the near field before strike-slip faulting. The postseismic strain accumulation implies a concentration of shear stress in the vicinity of the main fault plane. This stress concentration is induced by the postseismic anelastic flow in the underlying viscoelastic layers (YANG and TOKSÖZ, 1981) and will promote a long-term aftershock activity in the hypocentral region or creep-like secondary faulting in the near future.

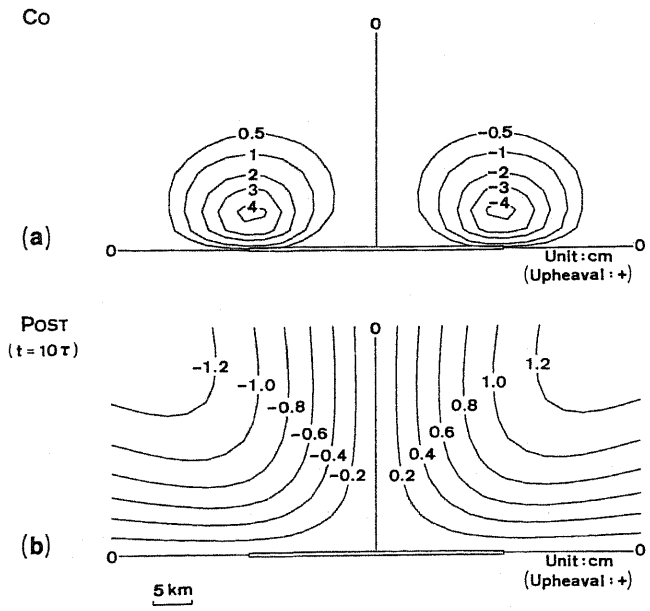

Fig. 8. Contour maps of (a) coseismic and (b) postseismic vertical displacements. See the caption of Fig. 7.

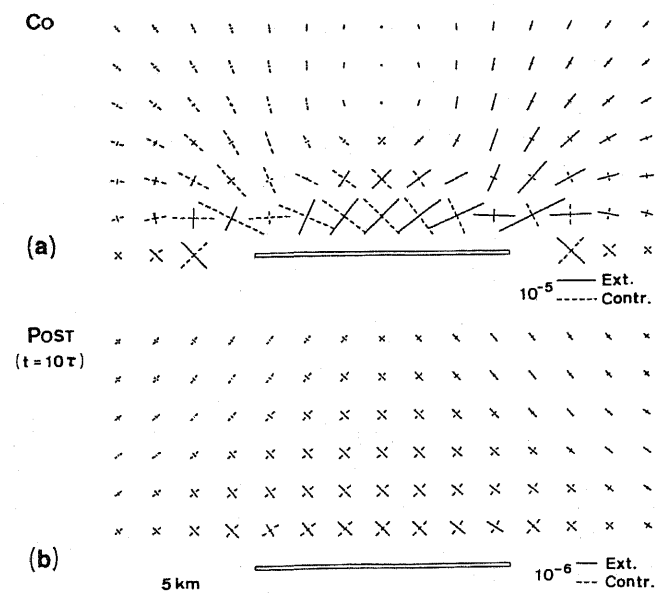

Fig. 9. (a) Coseismic and (b) postseismic horizontal strains. See the caption of Fig. 7.

3.3 Effect of viscoelastic structure

To estimate the effects of viscoelastic structure, horizontal displacements are calculated at five different elapsed times for three structure models with different viscosity ratios. Figure 10 shows the results, in which the profiles are taken along the line perpendicular to the center of the fault and the amount of displacement is normalized by U_0 that is the amount of dislocation on the fault plane. As shown in this figure, the variation in the viscosity ratio has a large effect on the amplitudes of the displacement profiles. As the viscosity ratio becomes smaller, which means that the viscosity of the lower crust decreases and approaches to that of the upper mantle, more remarkable deformation appears in the near field about 10 to 40 km away from the fault. In addition, it is noteworthy that the amplitude ratios among the profiles at different elapsed times are little changed in each structure model, while the amplitude itself is largely affected by the viscosity ratio.

Though the effect of viscoelastic structure on the surface deformation is remarkable as shown in Fig. 10, we cannot determine simultaneously the viscosity ratio η'/η and the relaxation time τ, even if a certain displacement profile is obtained. For example, it is difficult to recognize the difference between the profile obtained at $t=10\tau$ in the case of $\eta'/\eta=\infty$ and that obtained at $t=6\tau$ in the case of

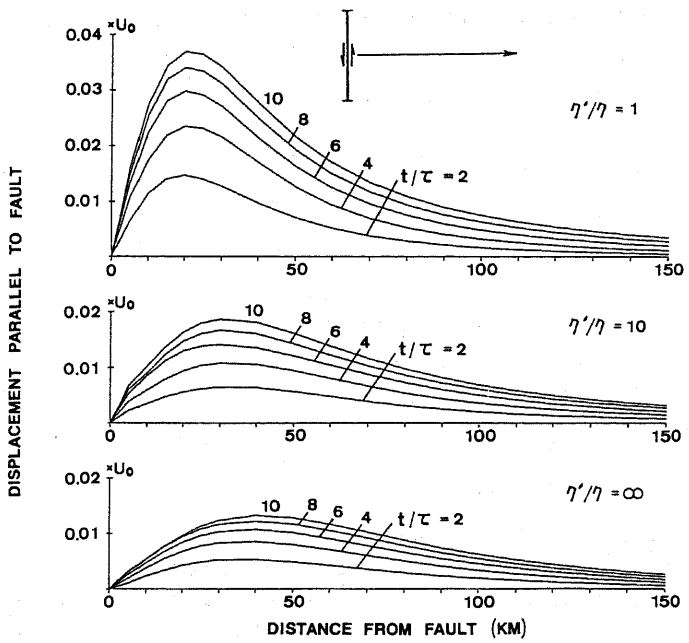

Fig. 10. Changes in horizontal displacement profiles with time for three structure models with different viscosity ratios. The profiles are taken along the line extending on the surface perpendicularly to the center of the fault. The scale of displacement is normalized by U_0. Parameters denoting the fault geometry are fixed at those in Figs. 7, 8, and 9.

$\eta'/\eta = 10$. Therefore, the measurement of postseismic deformation at long time intervals is not a powerful method for establishing a unique model for the viscoelastic structure of the earth's crust and upper mantle. For further information, long-term detailed monitoring of the deformation is indispensable and other kinds of field investigations are required. The value of the viscosity itself is discussed in connection with the time-dependence of deformation in the next subsection.

3.4 Time-dependence of deformation

Temporal variations in postseismic horizontal strains at selected positions are shown in Fig. 11. In this figure, changes in maximum shear strain due to pure strike-slip faulting with a dislocation of 3 m are plotted against the normalized elapsed time. The positions used for calculations are located perpendicular to the center of the fault. Viscosity ratio is assumed to be 10 as a representative value, which gives the deformation with moderate amplitude as shown in Fig. 10.

Figure 11 shows the continuation of viscoelastic deformation over a long time after faulting, being driven by the anelastic flow due to stress relaxation in the underlying viscoelastic layers. The apparent relaxation times at the surface are much longer than the rheological relaxation times of the underlying viscoelastic layers. This result is most likely due to a coupling of the elastic and viscoelastic

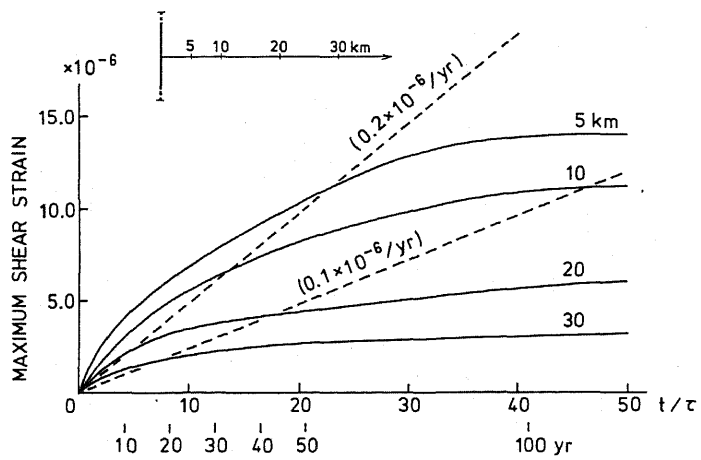

Fig. 11. Time changes in maximum shear strain due to strike-slip faulting with a dislocation of 3 m. The positions used for calculations are located perpendicular to the center of the fault. Parameters denoting the fault geometry are fixed at those in Figs. 7, 8, and 9. The viscosity ratio η'/η is assumed to be 10. Two broken straight lines approximate the stationary tectonic strain rates in the Inner Zone of Southwest Japan which are estimated by NAKANE (1973). These two lines and the elapsed times represented in years at the bottom of this figure are drawn under an assumption that the viscosity of the asthenosphere beneath Southwest Japan is 5×10^{19} P.

layers and is quite different from the treatment of the viscoelastic medium alone. The viscoelastic transient deformation reaches the nearly final steady state at the elapsed time $t \simeq 40\tau$. Converting the strain in final state into the displacement, the maximum displacement amounts to about 4% of that of the coseismic elastic deformation. Of course, this final value depends not only on the structure model but on the fault size and mode of faulting.

Two broken straight lines in Fig. 11 approximate the stationary tectonic strain rates in the Inner Zone of Southwest Japan, as estimated from the first-order triangulation by NAKANE (1973). It can be seen from this figure that the strain due to stress relaxation is dominant in the early stage of the postseismic deformation and that the postseismic strain field is gradually taken over by the tectonic strain with time.

The relaxation time of the asthenosphere, in other words, the viscosity and rigidity of the asthenosphere, must be evaluated to estimate the time-dependence of deformation quantitatively. It is unfavorable, however, that we have no available information concerning the value of viscosity of the asthenosphere beneath the Inner Zone of Southwest Japan. Thus we must assume viscosity from the studies that have been made for the Outer Zone of Southwest Japan or other region in the Japanese Islands.

The two broken straight lines in Fig. 11 and the elapsed times represented in years at the bottom of the figure are drawn under an assumption that the viscosity of the asthenosphere beneath the Japanese Islands is 5×10^{19} P (5×10^{18} Pa·s). This low viscosity has been mainly derived from a study by THATCHER and RUNDLE (1984) of the cyclic deformation caused by major underthrust earthquakes that periodically occur at the Nankai trough (Fig. 1). They modeled thrust faulting in a 30-km-thick elastic lithosphere overlying a viscoelastic asthenosphere. Moreover, this viscosity seems appropriate to explain the vertical movements observed after the 1923 Kanto earthquake of $M=7.9$ that occurred at the Sagami trough (Fig. 1) if the thickness of the lithosphere is 60 km (MATSU'URA and IWASAKI, 1983). More recently, MIYASHITA (1987) used 2×10^{20} P for the viscosity of the asthenosphere in a finite-element modeling of the cyclic deformations caused by underthrust earthquakes at the Nankai trough. The plate configuration and the layered structure of the model, however, are different from those of the model of THATCHER and RUNDLE (1984).

According to WALCOTT (1973), the viscosity of the asthenosphere as estimated from the analysis of postglacial uplifts depends on the thickness of the asthenosphere and lies in the wide range of from 10^{19} to 10^{21} P because the thickness, which is unknown, is somewhere between 100 and 500 km. This estimation has been made for shield regions that are considered to have a tectonically stable lithosphere with a thickness of about 110 km. For tectonically active inland regions, however, a thin lithosphere and a highly developed asthenosphere with low viscosity and sufficient thickness are expected. If we adopt viscosity of 5×10^{19} P, which is possibly the lower limit of the viscosity of the asthenosphere beneath the Japanese Islands, the relaxation time of the upper mantle is about 2.44 yr.

On the basis of these assumptions, we conclude that the viscoelastic deformation continues for about 100 years after faulting and the maximum of the cumulative strain until the final state amounts to about 15×10^{-6} in the vicinity of the fault; this can be easily verified by surface geodetic measurements. Here, it should be noted again that the postseismic strain is accumulated in the same sense as that of the tectonic strain. Therefore, a remarkable strain concentration can be expected on and in the vicinity of the fault plane if the same tectonic stress as that before faulting acts continuously on the region in question. However, the distinction of the postseismic strain from the whole strain field will become gradually more difficult with time because of the similarities of the two kinds of strain accumulation.

4. *Observations and Model Calculations*

The model of postseismic deformation due to stress relaxation is applied to the interpretation of crustal movements associated with a major earthquake in the Inner Zone of Southwest Japan.

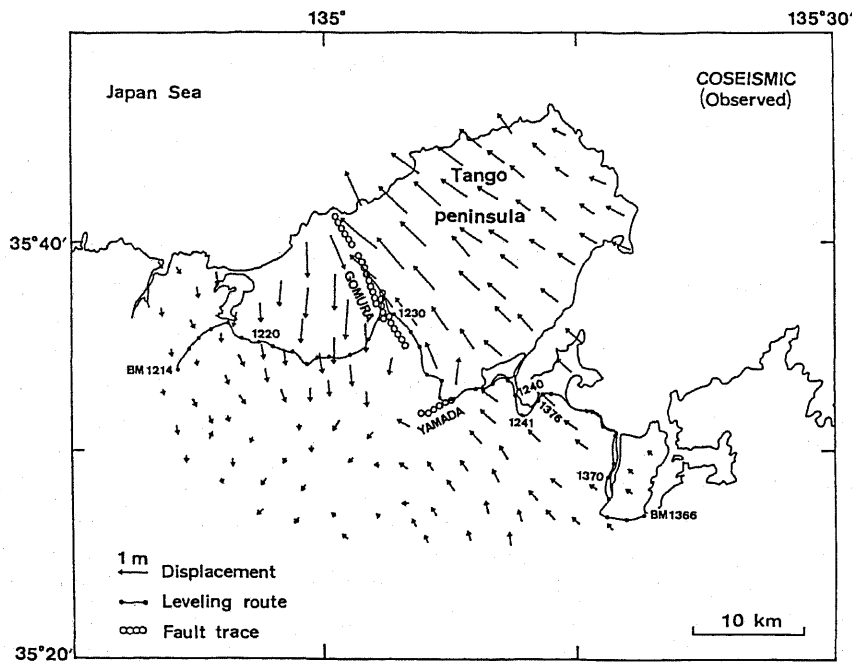

Fig. 12. Horizontal displacements at the triangulation points associated with the 1927 Tango earthquake of $M=7.5$. The data observed during the period from 1884–1889 to 1927, which were compiled by TSUBOI (1932), are employed. Numerals attached to the leveling route indicate the identity numbers of bench marks.

4.1 The 1927 Tango earthquake

The 1927 Tango earthquake of $M=7.5$ is probably one of the best geodetically documented earthquakes in the Inner Zone and most appropriate for examining the deformation due to postseismic stress relaxation. The epicenter and mechanism diagram are shown in Fig. 2.

The 1943 Tottori and 1948 Fukui earthquakes seem less appropriate in examining the postseismic deformation than the Tango earthquake. The revision survey for the Tottori earthquake was carried out about 14 years after the earthquake (SATO, 1973). This seems too long to distinguish coseismic and postseismic deformations from the measurements. Moreover, it is uncertain how much the thick alluvial layer in the Fukui region (NASU, 1950) affected the surface deformation. And more unfortunately, the resurveyed regions after these two earthquakes are smaller than in the case of the Tango earthquake.

Two remarkable seismic faults (the Gomura and Yamada faults), which are conjugate to each other, appeared at the time of the Tango earthquake. Detailed investigations of crustal movements associated with this earthquake were made by TSUBOI (1930 a, b, 1931, 1932). Figure 12 shows the horizontal displacements at the 137 triangulation points during the period from 1884–1889 to 1927. The pattern of the displacements reveals large left-lateral strike-slip movements along the Gomura fault and slightly right-lateral ones across the Yamada fault. Vertical displacements during the period from 1888 to 1927 along the first-order leveling route, which is shown in Fig. 12, are plotted in Fig. 13. A large dip-slip movement of over 1 m is seen across the Yamada fault while the movement across the Gomura

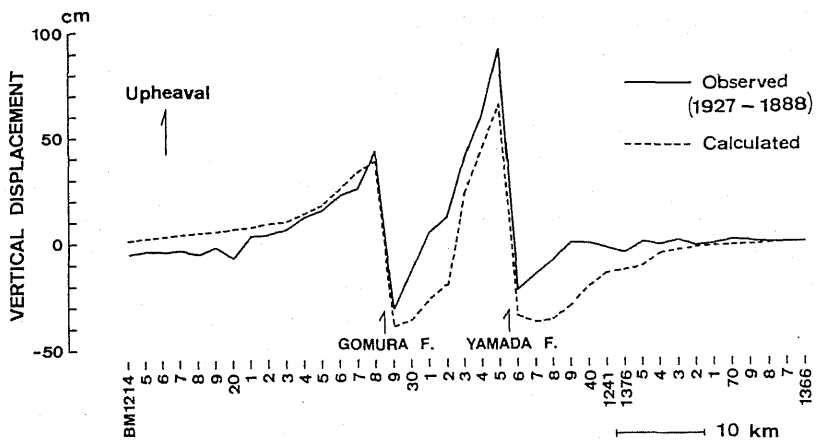

Fig. 13. Changes in relative heights of bench marks along the first-order leveling route. The solid and broken lines indicate the observed and calculated vertical displacements, respectively. Bench mark 1366 is assumed to be a datum point. The observed data were compiled by TSUBOI (1930 a). Fault models adopted for the calculation are given in Table 3 and the locations of bench marks are shown in Fig. 12.

fault is about 0.7 m that is smaller than the strike-slip one.

The distribution of aftershocks was investigated in detail by NASU (1935). Most of the aftershocks immediately following the main shock are shallower than 20 km and generally distributed along the fault traces. He concluded that the Gomura fault is nearly vertical (or steeply inclined southwestward) while the Yamada fault dips northwestward at an angle of about 50°.

Studies to establish fault models from geodetic data have been made to interpret the crustal movements observed (KASAHARA, 1957; CHINNERY, 1961; WALSH, 1969; MATSU'URA, 1977; MATSU'URA and IWASAKI, 1982). On the other hand, KANAMORI (1973) calculated synthetic seismograms by varying fault parameters and has established a seismological model for the Gomura fault that best fits the observed seismogram.

According to these geodetic and seismological studies, the fault parameters of the Gomura fault are generally as follows (see Fig. 4(b) for definitions of the parameters): $L=30$–35 km, $W=10$–19 km, $U_0=3.0$–3.7 m, and λ takes a small value indicating a predominantly left-lateral strike-slip. The fault plane is considered nearly vertical though there are a few discrepancies among the models about the dip direction. The fault parameters of the Yamada fault are generally as follows: $L=10$–15 km, $W=9$–20 km, $U_0=1.3$–1.8 m, $\lambda\simeq 120°$ (reverse faulting with a right-lateral strike-slip component), and $\delta=40$–$60°$.

In the present study, a simple fault model with a uniform dislocation on the fault plane is adopted because the main purpose of the present study is not to discuss the spatial variations of fault parameters but to comprehend spatial and temporal modes of postseismic transient deformation. The fault parameters of the Tango earthquake adopted in the present study are listed in Table 3. Taking the aftershock distribution into consideration, the dip-angle of the Gomura fault is fixed at 90°. Other parameters have been obtained after some modification of the pre-existing models.

Coseismic displacements have been calculated using the structure model listed in Table 2 and the fault models in Table 3. Horizontal displacements calculated are shown in Fig. 14 and vertical ones are plotted in Fig. 13 superposed with the observed profile. The calculated crustal movements generally agree well with the observed ones, indicating that a simple model with a uniform dislocation is sufficiently effective as a first approximation to interpret the mode of faulting.

As shown in Figs. 12 and 14, small discrepancies between the observed and

Table 3. Fault parameters of the 1927 Tango earthquake adopted for the calculations.

Fault	L (km)	W (km)	D (km)	δ (°)	U_0 (m)	λ (°)	strike (°)*
Gomura	35	15	15.2	90	3.0	15	153
Yamada	12	10	8.8	60	1.5	130	243

* Measured clockwise from north, with the fault dipping down to the right of the strike direction.

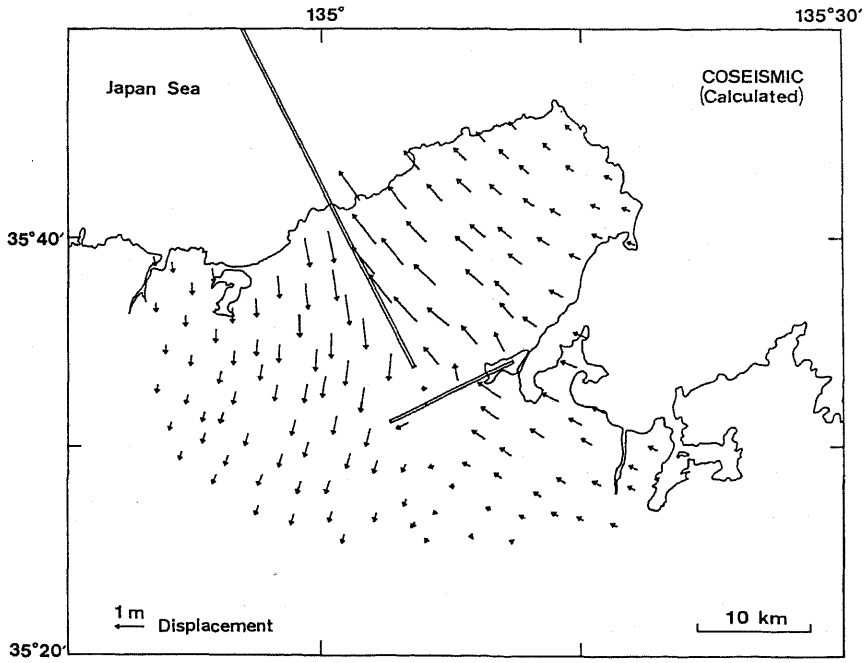

Fig. 14. Calculated coseismic horizontal displacements. Points selected for calculations coincide with the triangulation points shown in Fig. 12. Fault models are the same as those employed in Fig. 13.

calculated crustal movements are recognized in the southwestern part of the region and also in the head region of the Tango Peninsula. In the former case, the effects of the 1925 Tajima earthquake of $M=7.0$, which occurred at about 25 km west of and about 21 months before the Tango earthquake, may be present. In the latter case, however, the cause of discrepancy is not known. There might be systematic errors due to movements of reference points which are not considered here. Nevertheless, we consider that these discrepancies are small and negligible compared with the general agreement of the calculated crustal movements with the observed ones.

4.2 Postseismic deformation due to stress relaxation

In reality, repeated geodetic surveys to detect horizontal deformations are laborious tasks, and it is unfortunate that the interval between consecutive surveys is too long to grasp the progress of crustal movements in detail in most cases of strike-slip faulting. Figure 15 shows the horizontal strains produced in the 52 years following the 1927 Tango earthquake (GEOGRAPHICAL SURVEY INSTITUTE, 1987). The deformation is generally characterized by a contraction in an almost E-W to ESE-WNW direction with a strain rate of about $0.2\text{–}0.3 \times 10^{-6}$/yr. This strain field has probably been caused not only by the postseismic viscoelastic deformation

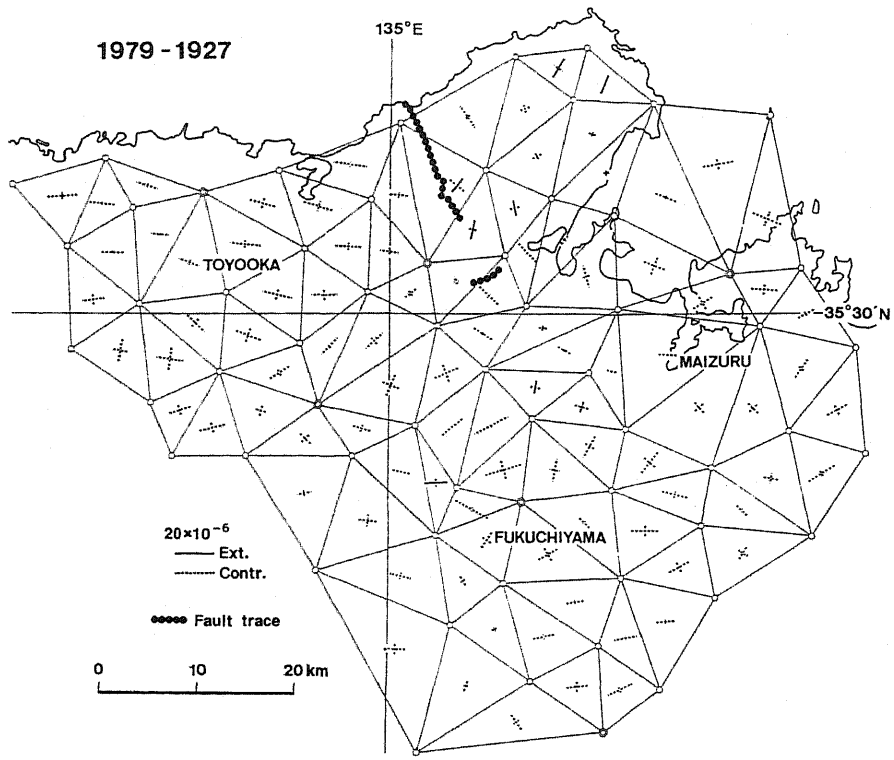

Fig. 15. Horizontal strains in Tango district produced in the 52 years following the 1927 Tango earthquake (compiled from GEOGRAPHICAL SURVEY INSTITUTE, 1987).

associated with the 1927 Tango earthquake but also by the regional tectonic stress, which is characterized by a compression in the same direction. The latter is considered to make a larger contribution than the former because strains at positions sufficiently apart from the faults are nearly comparable to those in the near field of the fault. The strain field in the Tango Peninsula is somewhat out of harmony with the others. This is noteworthy because there are also quantitative discrepancies between the observed and calculated coseismic displacements in the Tango Peninsula (Figs. 12 and 14).

For the calculations of postseismic viscoelastic deformation, we assume 5×10^{19} P for the viscosity of the upper mantle. This value of the viscosity has been derived from studies of the postseismic deformation in Japan, as discussed in Sec. 3. The relaxation time τ, as derived from the above viscosity, is 2.44 yr. Therefore, the time of the latest survey shown in Fig. 15 corresponds to an elapsed time of about 21τ after the earthquake. On the contrary, there is little information about the viscosity ratio η'/η. We tentatively assume $\eta'/\eta = 10$, a value which gives

the deformation with a moderate amplitude, as shown in Fig. 10, but can be modified later. Here, it should be noted that varying the viscosity ratio affects the amplitude of deformation but has little effect on the deformation pattern.

The postseismic viscoelastic deformation during the period corresponding to that shown in Fig. 15 is calculated for 132 mesh points at intervals of 4 km. The contributions from the Gomura and Yamada faults are superposed, though, because of its size, the effect of the Yamada fault is comparatively small. The horizontal displacement field is quite similar to the model result shown in Fig. 7(b), that is considered to directly reflect the pattern of tectonic flow induced in the underlying viscoelastic layers. In contrast, the vertical displacement field, not shown here, indicates a pattern which is quite different from that shown in Fig. 8(b). This is chiefly because of the dip-slip component of the Gomura fault and partly because of the existence of the Yamada fault.

Though the general features of the calculated horizontal strain field shown in Fig. 16 are in harmony with the observed ones shown in Fig. 15, there are a few discrepancies. The calculated strains are smaller than those observed. The distribution of extension is comparable with that of contraction in the calculated strain field, while extension is hardly observed except in the Tango Peninsula. Moreover, a

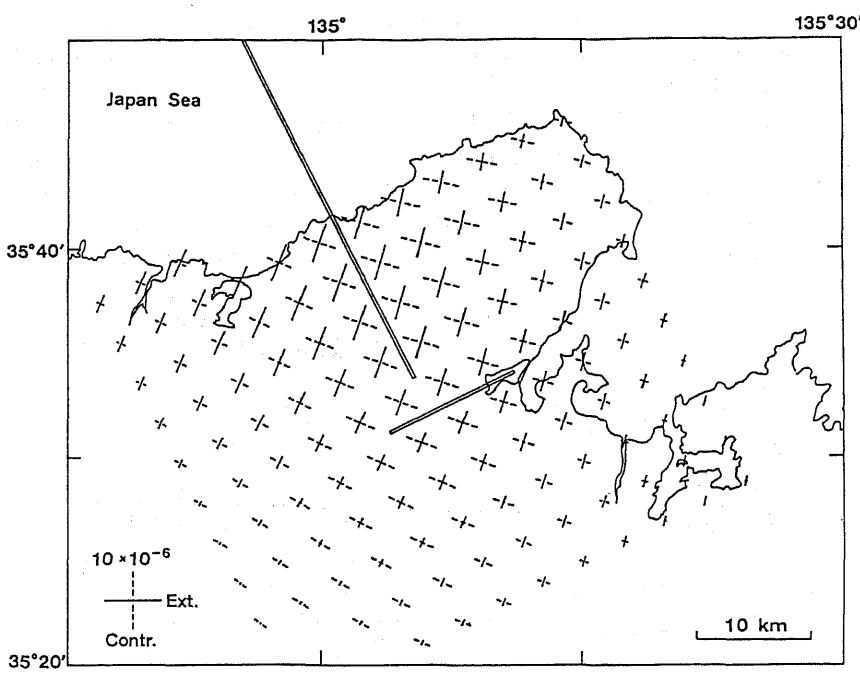

Fig. 16. Calculated postseismic horizontal strains associated with the 1927 Tango earthquake. Calculation has been made at $t=21\tau$, that almost corresponds to the time of the latest survey shown in Fig. 15, assuming $\eta=5\times10^{19}$ P and $\eta'/\eta=10$.

strain concentration near the faults is seen in the calculated strain field but not in the observed one. Quantitative discrepancies between the observed and calculated strain fields can be reduced to some extent if we decrease the viscosity of the lower crust and make it approach to that of the upper mantle, or if we adopt a smaller value for the viscosity of the upper mantle keeping the viscosity ratio fixed. However, the discrepancy between deformation patterns remains mostly unchanged. Thus it is supposed that the observed strain field shown in Fig. 15 is most likely due to the effect of superposition of the postseismic viscoelastic deformation associated with the 1927 Tango earthquake and the tectonic stress acting on the region after the earthquake.

5. *Discussion*

Figure 17 shows coseismic and postseismic changes in relative height between two adjacent bench marks with a distance of about 2 km across the Gomura and Yamada faults (KANAMORI, 1973). The movement across the Gomura fault is relatively small and its rate decayed rapidly within a few years after the earthquake. In contrast, the movement across the Yamada fault has shown a gradual progress that can be fitted by an exponential function with a time constant of about 3.0 yr.

As seen in Fig. 8(b), postseismic vertical displacement is hardly detectable by geodetic measurements in the short distance across the vertical strike-slip fault. In the case of the Gomura fault, which has a coseismic dip-slip component of about 0.8 m, calculated postseismic relative displacement between the bench marks above is, at most, smaller than a few millimeters. Moreover, it is in the reverse sense to that of the observed movement shown in Fig. 17 and has a much longer time constant. On the other hand, the pattern of postseismic deformation around the inclined dip-slip fault is largely dependent on the dip angle and width of the fault plane

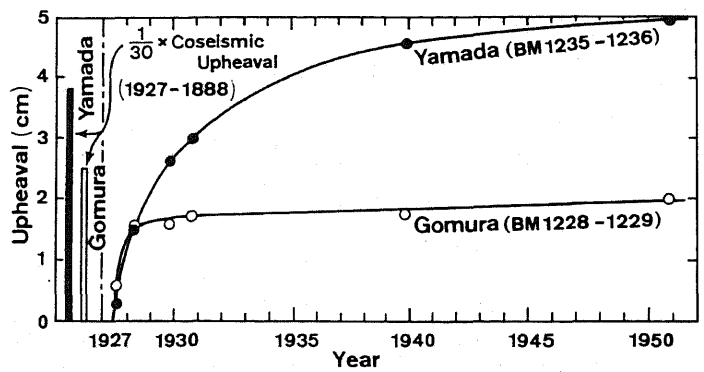

Fig. 17. Coseismic and postseismic changes in relative height between two adjacent bench marks with a distance of about 2 km across the Gomura and Yamada faults (after KANAMORI, 1973). The postseismic change until 1930 was first pointed out by TSUBOI (1931).

(THATCHER *et al.*, 1980). Relative displacement calculated for the Yamada fault shows a better agreement with the observation than for the Gomura fault. However, the relative displacement does not exceed 1 cm even in three decades after the earthquake; this is far smaller than the observed movement. Therefore, we infer that the creep-like movements shown in Fig. 17 were not the viscoelastic deformation caused by postseismic stress relaxation.

It is noticed that these creep-like movements progressed in the same sense as that in the coseismic movements. This implies that these movements were caused under stress state similar to the regional tectonic stress. Though there still remains a possibility that the occurrence of the earthquake caused a new stress concentration around the faults, it is expected that the tectonic stress has continued acting in the region concerned and dominating the regional crustal movements even after the earthquake.

We cannot, unfortunately, determine which parts of the fault plane underwent such creep-like motions. However, the duration and final amount of motion were probably dependent on the non-uniform distribution of frictional strengths on the fault plane, as pointed out by MIKUMO and MIYATAKE (1979). While the long-term creep-like movements are represented by exponential functions, there is no information about the short-term behavior on the fault plane. There is a possibility that the cumulative displacement curves shown in Fig. 17 consist of a series of episodic creeps in the manner similar to the creep motions on the San Andreas fault (SMITH and WYSS, 1968).

The postseismic creep-like motion will induce an additional, though probably slight, deformation in the surroundings of the fault. This additional deformation consists of an elastic part responding to the gradual slip on the fault plane and a transient viscoelastic part. Both parts are time-dependent in this case, though the viscoelastic part is small enough to be neglected. The patterns of the elastic part of the additional deformation are quite similar to those of the elastic deformation at the time of earthquake, except in the amount and the time-dependence. In the present study, this additional deformation cannot be taken into the model of postseismic deformation, since there is no information about the size and location of the plane where the creep-like motion occurred. However, it is noticed that the horizontal strain in the elastic part of the additional deformation will be accumulated in the same sense as that of the coseismic strain release; in other words, in the nearly reverse sense to that of the postseismic viscoelastic strain accumulation. This is inferred from the comparison of Fig. 9(a) with Fig. 9(b). Therefore, the strain concentration near the fault will be somewhat reduced by the additional strain in the reverse sense.

Considering the contribution of regional tectonic stress, we introduce uniform regional strains into the postseismic strain field. Here, we assume contraction of 0.16×10^{-6}/yr in the ESE-WNW direction and perpendicular extension of 0.04×10^{-6}/yr on the basis of the three following observations: the stationary tectonic strain rate of about 0.2×10^{-6}/yr in maximum shear (NAKANE, 1973), the

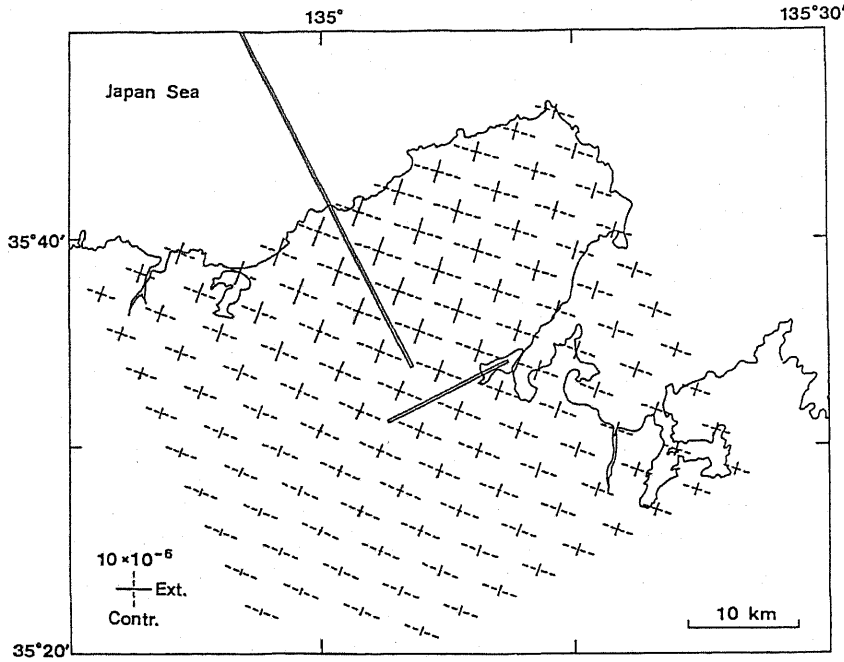

Fig. 18. Calculated postseismic horizontal strains with the uniform regional strain superposed. The regional strain is assumed to consist of contraction with a rate of 0.16×10^{-6}/yr in the ESE-WNW direction and extension with a rate of 0.04×10^{-6}/yr in the perpendicular direction to that of the contraction.

strain observed at the positions sufficiently apart from the fault as shown in Fig. 15, and the strikes of the Gomura and Yamada faults. Figure 18 shows the calculated postseismic strain field, where the uniform regional strains are superposed on the postseismic viscoelastic ones shown in Fig. 16. The additional deformation due to a postseismic creep-like motion is not considered. This figure shows a better agreement with the observed results shown in Fig. 15, though the discrepancy in the Tango Peninsula remains little improved.

Figure 18 also indicates the difficulties in understanding and distinguishing the effects of the deformation caused by postseismic stress relaxation from the strain fields observed. This is because the pattern of the postseismic viscoelastic strain fields is quite similar to that of the regional tectonic strain. To remove the ambiguity resulting from the similarities and to distinguish between these two types of deformations, a long-term detailed monitoring of postseismic crustal movements is indispensable in the region extending to about 100 km from the fault. This is because remarkable postseismic displacement will appear in the near field about 15 to 40 km away from the fault, as shown in Fig. 10. Unfortunately, such monitoring has not yet been accomplished, mainly because of the shortage of measurements

resulting from the laborious tasks involved in repeated geodetic surveys and partly because of a lack of accuracy. However, we are convinced that these problems will be overcome in the near future by employing a new and more accurate method with a simpler management; for example, by three-dimensional relative positionings using the Global Positioning System (GPS) engaged in advanced space techniques.

According to YAMAUCHI (1975), the apparent relaxation times of the postseismic deformations detected by continuous observations of crustal movements or geodetic measurements range from about 20 min to about 8 yr, though not all of the deformations accompanied earthquakes of strike-slip fault type. The remarkable postseismic deformation with its small relaxation time, that is often detected by continuous observations with strainmeters or tiltmeters, cannot be explained by stress relaxation in the underlying viscoelastic layers. Therefore, another deformation mechanism should be considered. TANAKA (1981) has concluded that some of the deformation with a time constant of a few years may be caused by viscoelastic stress relaxation within rocks around the observation vault. Moreover, it is supposed that the earthquake-induced transient movements of underground water sometimes have large effects on local surface deformations during the period immediately after an earthquake (TABEI, 1987). The mechanism of the postseismic deformation that originates from the superficial layer of the crust, however, has not been considered in the present study. To understand the nature of the crust, more details of the mechanism of postseismic deformation should be investigated.

6. *Concluding Remarks*

Transient deformation caused by postseismic stress relaxation in underlying viscoelastic layers is examined through a three-dimensional numerical simulation mainly for strike-slip faulting in the Inner Zone of Southwest Japan. In the present model, viscoelastic treatments are introduced to the upper mantle and also to the lower crust on the basis of the depth distribution of hypocenters of microearthquakes in the region concerned.

It is made clear that the fault size as well as the viscoelastic structure of the earth's crust and upper mantle has a large effect on the amount of postseismic deformation. Thus the fault size should be taken into serious consideration in modeling the faulting.

The most noteworthy result in the model calculations is the distribution patterns of the postseismic strain field. A large shear strain, which is similar to the preseismic strain accumulation and is contrary to the coseismic strain release, is induced for a long time after faulting in the near field of the fault zone. The viscoelastic structure of the earth's crust and upper mantle, however, is hard to determine solely on the basis of geodetic measurements executed at long time intervals. Therefore, a long-term detailed monitoring of the deformation is indispensable and other kinds of field investigations are required to obtain further information about the viscoelastic structure.

Crustal movements associated with the 1927 Tango earthquake of $M=7.5$ are examined for both the coseismic elastic rebound and the postseismic viscoelastic transient deformation caused by stress relaxation after faulting. The coseismic movements can be fitted by a simple conjugate fault system in which a uniform dislocation on the fault plane is assumed. The discrepancies between the observed and calculated postseismic movements are most likely due to the effect of tectonic stress. The tectonic stress is considered to have continued acting and dominating the regional crustal movements even after the earthquake.

The ambiguity resulting from the similarities between the deformation due to postseismic stress relaxation and the regional tectonic movements remains unsolved. But we are convinced that it will be overcome by long-term detailed monitoring of the movements employing a new technique with a higher accuracy and a simpler management; for example, by three-dimensional relative positionings using the Global Positioning System, in the near future.

I would like to thank Professor Ichiro Nakagawa for giving helpful advice throughout the course of this study and critically reading the manuscript. I wish also to acknowledge the valuable discussions with Professor Norihiko Sumitomo, Mr. Yutaka Tanaka, Mr. Kunio Fujimori, and the members of our laboratory. My thanks are also due to Professors Yoshimichi Kishimoto, Takeshi Mikumo, Torao Tanaka, and Kazuo Oike, who kindly offered helpful comments for the revision of the manuscript.

The numerical calculations were executed with the computer system at the Data Processing Center of Kyoto University.

REFERENCES

ANDO, M., Source mechanisms and tectonic significance of historical earthquakes along the Nankai trough, Japan, *Tectonophysics*, **27**, 119–140, 1975.

ANDREWS, D. J. and N. H. SLEEP, Numerical modelling of tectonic flow behind island arcs, *Geophys. J. R. Astron. Soc.*, **38**, 237–251, 1974.

CHEN, W. and P. MOLNAR, Focal depths of intracontinental and intraplate earthquakes and their implications for the thermal and mechanical properties of the lithosphere, *J. Geophys. Res.*, **88**, 4183–4214, 1983.

CHINNERY, M. A., The deformation of the ground around surface faults, *Bull. Seismol. Soc. Am.*, **51**, 355–372, 1961.

GEOGRAPHICAL SURVEY INSTITUTE, Horizontal strain in Japan 1985–1883, Technical Data F. 1-No. 6 in Geographical Survey Institute, 133 pp., 1987.

HASHIDA, T. and K. SHIMAZAKI, Determination of seismic attenuation structure and source strength by inversion of seismic intensity data: Tohoku district, Northeastern Japan, *J. Phys. Earth*, **35**, 67–92, 1987.

HASHIMOTO, M., Numerical modelling of the three-dimensional stress field in southwestern Japan, *Tectonophysics*, **84**, 247–266, 1982.

HIRAHARA, K., Three-dimensional seismic structure beneath Southwest Japan: The subducting Philippine Sea plate, *Tectonophysics*, **79**, 1–44, 1981.

HUZITA, K., Y. KISHIMOTO, and K. SHIONO, Neotectonics and seismicity in the Kinki area,

Southwest Japan, *J. Geosci. Osaka City Univ.*, **16**, 93–124, 1973.

ICHIKAWA, M., Reanalyses of mechanism of earthquakes which occurred in and near Japan, and statistical studies on the nodal plane solutions obtained, 1926–1968, *Geophys. Mag. Jpn. Meteorol. Agency*, **35**, 207–274, 1971.

ITO, K., Depth of seismicity and its relation to thermal structure and large intra-plate earthquakes in northern Kinki district, Japan, *Rep. Meet. Stud. Earthq. Predict. Kyoto Univ.*, **17**, 6–18, 1988 (in Japanese).

IWASAKI, T., Quasi-static deformation due to a dislocation source in a Maxwellian viscoelastic earth model, *J. Phys. Earth*, **33**, 21–43, 1985.

IWASAKI, T. and M. MATSU'URA, Quasi-static crustal deformations due to a surface load: Rheological structure of the earth's crust and upper mantle, *J. Phys. Earth*, **30**, 469–508, 1982.

KANAMORI, H., Mantle beneath the Japanese arc, *Phys. Earth Planet. Inter.*, **3**, 475–483, 1970.

KANAMORI, H., Tectonic implications of the 1944 Tonankai and the 1946 Nankaido earthquakes, *Phys. Earth Planet. Inter.*, **5**, 129–139, 1972 a.

KANAMORI, H., Determination of effective tectonic stress associated with earthquake faulting, The Tottori earthquake of 1943, *Phys. Earth Planet. Inter.*, **5**, 426–434, 1972 b.

KANAMORI, H., Mode of strain release associated with major earthquakes in Japan, *Ann. Rev. Earth Planet. Sci.*, **1**, 213–239, 1973.

KASAHARA, K., The nature of seismic origins as inferred from seismological and geodetic observations (1), *Bull. Earthq. Res. Inst., Univ. Tokyo*, **35**, 473–532, 1957.

KOBAYASHI, Y., A relationship between the distribution of focal depth of microearthquakes and surface heat flow in the southwestern Japan and central Japan, Proc. Earthq. Predict. Res. Symp., 184–193, 1976 (in Japanese).

MATSU'URA, M., Inversion of geodetic data. Part II. Optimal model of conjugate fault system for the 1927 Tango earthquake, *J. Phys. Earth*, **25**, 233–255, 1977.

MATSU'URA, M. and T. IWASAKI, Analysis of geodetic data by using a new inversion technique. Redetermination of fault model of the 1927 Kita-Tango earthquake, Prog. Abstr. Seismol. Soc. Jpn., No. 1, 1, 1982 (in Japanese).

MATSU'URA, M. and T. IWASAKI, Study on coseismic and postseismic crustal movements associated with the 1923 Kanto earthquake, *Tectonophysics*, **97**, 201–215, 1983.

MATSU'URA, M., T. TANIMOTO, and T. IWASAKI, Quasi-static displacements due to faulting in a layered half-space with an intervenient viscoelastic layer, *J. Phys. Earth*, **29**, 23–54, 1981.

MEISSNER, R. and J. STREHLAU, Limits of stresses in continental crust and their relation to the depth-frequency distribution of shallow earthquakes, *Tectonics*, **1**, 73–89, 1982.

MIKUMO, T. and T. MIYATAKE, Earthquake sequences on a frictional fault model with non-uniform strengths and relaxation times, *Geophys. J. R. Astron. Soc.*, **59**, 497–522, 1979.

MIKUMO, T., H. WADA, and M. KOIZUMI, Seismotectonics of the Hida region, central Honshu, Japan, *Tectonophysics*, **147**, 95–119, 1988.

MIYASHITA, K., Surface displacement patterns associated with asthenospheric stress relaxation following major underthrust earthquakes, *Zisin* (*J. Seismol. Soc. Jpn.*), **36**, 541–550, 1983 (in Japanese).

MIYASHITA, K., A model of plate convergence in Southwest Japan, inferred from leveling data associated with the 1946 Nankaido Earthquake, *J. Phys. Earth*, **35**, 449–467, 1987.

MIZOUE, M., Some remarks on the characteristics of subcrustal earthquake activities, Proc.

Earthq. Predict. Res. Symp., 97–105, 1976 (in Japanese).
NAKANE, K., Horizontal tectonic strain in Japan (II), *J. Geod. Soc. Jpn.*, **19**, 200–208, 1973 (in Japanese).
NAKANISHI, I., Precursors to ScS phases and dipping interface in the upper mantle beneath Southwestern Japan, *Tectonophysics*, **69**, 1–35, 1980.
NASU, N., Supplementary study on the stereometrical distribution of the after-shocks of the great Tango earthquake of 1927, *Bull. Earthq. Res. Inst., Univ. Tokyo*, **13**, 335–399, 1935.
NASU, N., Crustal deformation, in *The Fukui Earthquake of June 28, 1948*, ed. Committee for the Study of Fukui Earthquake, pp. 93–130, Tokyo, 1950.
NISHIDA, R., Earthquake generating stress in eastern Chugoku and northern Kinki districts, Southwest Japan, *Bull. Disas. Prev. Res. Inst., Kyoto Univ.*, **22**, 197–233, 1973.
NUR, A. and G. MAVKO, Postseismic viscoelastic rebound, *Science*, **183**, 204–206, 1974.
OIKE, K., Seismic activities and crustal movements at the Yamasaki fault and surrounding regions in the Southwest Japan, *J. Phys. Earth*, **25**, Suppl., S31–S41, 1977.
RUNDLE, J. B. and D. D. JACKSON, A three-dimensional viscoelastic model of a strike slip fault, *Geophys. J. R. Astron. Soc.*, **49**, 575–591, 1977.
SATO, H., A study of horizontal movement of the earth crust associated with destructive earthquakes in Japan, *Bull. Geograph. Surv. Inst.*, **19**, 89–130, 1973.
SATO, K., H. ISHII, and A. TAKAGI, Characteristics of crustal stress and crustal movements in the northeastern Japan arc. I: Based on the computation considering the crustal structure, *Zisin (J. Seismol. Soc. Jpn.)*, **34**, 551–563, 1981 (in Japanese).
SAVAGE, J. C. and W. H. PRESCOTT, Asthenospheric readjustment and the earthquake cycle, *J. Geophys. Res.*, **83**, 3369–3376, 1978.
SHIONO, K., Focal mechanisms of major earthquakes in Southwest Japan and their tectonic significance, *J. Phys. Earth*, **25**, 1–26, 1977.
SIBSON, R. H., Fault zone models, heat flow, and the depth distribution of earthquakes in the continental crust of the United States, *Bull. Seismol. Soc. Am.*, **72**, 151–163, 1982.
SMITH, S. W. and M. WYSS, Displacement on the San Andreas fault subsequent to the 1966 Parkfield earthquake, *Bull. Seismol. Soc. Am.*, **58**, 1955–1973, 1968.
TABEI, T., On the postseismic deformation at Ikuno immediately after the 1984 Yamasaki earthquake, *J. Phys. Earth*, **35**, 225–239, 1987.
TANAKA, T., On the viscoelastic changes appearing on tiltmetric and extensometric records of the ground, *J. Geod. Soc. Jpn.*, **27**, 225–238, 1981.
THATCHER, W. and J. B. RUNDLE, A model for the earthquake cycle in underthrust zones, *J. Geophys. Res.*, **84**, 5540–5556, 1979.
THATCHER, W. and J. B. RUNDLE, A viscoelastic coupling model for the cyclic deformation due to periodically repeated earthquakes at subduction zones, *J. Geophys. Res.*, **89**, 7631–7640, 1984.
THATCHER, W., T. MATSUDA, T. KATO, and J. B. RUNDLE, Lithospheric loading by the 1896 Riku-u earthquake, Northern Japan: Implications for plate flexure and asthenospheric rheology, *J. Geophys. Res.*, **85**, 6429–6435, 1980.
THE RESEARCH GROUP FOR ACTIVE FAULTS, *Active Faults in Japan*, the University of Tokyo Press, Tokyo, 239 pp., 1980 (in Japanese).
TSUBOI, C., Investigation on the deformation of the earth's crust in the Tango district connected with the Tango earthquake of 1927 (Part I), *Bull. Earthq. Res. Inst., Univ. Tokyo*, **8**, 153–221, 1930 a.

TSUBOI, C., Investigation on the deformation of the earth's crust in the Tango district connected with the Tango earthquake of 1927 (Part II), *Bull. Earthq. Res. Inst., Univ. Tokyo*, **8**, 338–345, 1930 b.

TSUBOI, C., Investigation on the deformation of the earth's crust in the Tango district connected with the Tango earthquake of 1927 (Part III), *Bull. Earthq. Res. Inst., Univ. Tokyo*, **9**, 423–434, 1931.

TSUBOI, C., Investigation on the deformation of the earth's crust in the Tango district connected with the Tango earthquake of 1927 (Part IV), *Bull. Earthq. Res. Inst., Univ. Tokyo*, **10**, 411–434, 1932.

WALCOTT, R. I., Structure of the earth from glacio-isostatic rebound, *Ann. Rev. Earth Planet. Sci.*, **1**, 15–37, 1973.

WALSH, J. B., Dip angle of faults as calculated from surface deformation, *J. Geophys. Res.*, **74**, 2070–2080, 1969.

YAMAUCHI, T., On the elastic after-effect associated with earthquake, *J. Geod. Soc. Jpn.*, **21**, 75–80, 1975 (in Japanese).

YANG, M. and M. N. TOKSÖZ, Time-dependent deformation and stress relaxation after strike slip earthquakes, *J. Geophys. Res.*, **86**, 2889–2901, 1981.

YOSHII, T., Y. SASAKI, T. TADA, H. OKADA, S. ASANO, I. MURAMATU, M. HASHIZUME, and T. MORIYA, The third Kurayosi explosion and the crustal structure in the western part of Japan, *J. Phys. Earth*, **22**, 109–121, 1974.